Journal of Engineering and Development, Vol. 12, No. 4, December (2008) ISSN 1813-7822

Design of a Dynamometer for High Power Engines

Asst. Prof. Dr. Ibrahem A. Muhsin
Mechanical Engineering Department
University of Technology, Baghdad, Iraq

Asst. Prof. Dr. Jawad K. Oleiwi
Materials Engineering Department
University of Technology, Baghdad, Iraq

Abstract

This study is conducted to design a hydraulic dynamometer to assay a high power engines by employing the tapered land thrust bearing for absorbing engine power. The project is an attempt to design a dynamometer device, which could be used in the libratory of industries.

The design work involves a theoretical approach based on finite element analysis for the main parts of this hydraulic dynamometer which are the spline hollow shaft, the tapered–land thrust bearing and selection oil cooling system.

The results show that the shaft length = 0.6 m and diameter ratio (D_o/D_i) =1.5 for outer diameter D_o= 0.1524 m with 18–spline teeth which represents the hollow splined shaft. While for the thrust bearing the diameter ratio (d_o/d_i) =1.28 for inner diameter d_i = 0.1778 m and bearing thickness = 4 mm with numbers of bearing pairs = 40 and using oil type VG 22 as lubricant fluid with dynamic viscosity = 13 cp at 50 °C.

الخلاصـــــــة

أن هذه الدراسة هي مشروع لتصميم جهاز قياس قدرة هايدروداينميكي لقياس قدرة المحركات ذات القدرة العالية وذالك بتوظيف المساند الدفعية الهيدروداينميكية لامتصاص تلك القدرة. حيث يحاول هذا البحث تصميم جهاز قياس القدرة الذي يمكن استخدامه في مختبرات المصانع الفحصية.

يتضمن العمل التصميمي البحث النظري واستخدام العناصر المحددة لتحليل الأجزاء المهمة في جهاز قياس القدرة الهيدروداينميكي والمتمثلة بكل من عمود الإدارة المجوف وكذلك المساند الهيدروداينميكية الدفعية ومن ثم اختيار منظومة تبريد الزيت المناسبة.

لقد بينت النتائج النهائية للتصميم بان طول عمود الإدارة (L = 0.6 m) ونسبة الأقطار (shaft diameter ratio Do/Di =1.5) لقطر خارجي (D_o = 0.1524 m) ويحتوي على أسنان خارجية (spline teeth = 18) لأفضل نموذج. بينما وجد إن نسبة الأقطار للمسند الهيدروداينميكي الدفعي (disk diameter ratio d_o/d_i = 1.28) لقطر داخلي (d_i = 0.1778 m) وبأسنان داخلية عدد ١٨ وسمك القرص (t = 4 mm) وان عدد أزواج المسند (numbers of bearing pairs = 40). حيث استخدم زيت نوع (VG 22) بلزوجة (Z = 13 centipoise) في درجة حرارة 50 °C.

1. Introduction

1-1 General

A dynamometer is an instrument for determining power, usually by the independent measurement of force, time, and distance through which the force is moved, Land and Taylor [1, 2].

Absorption-hydraulic dynamometers are used primarily in very large engines, where the power absorbing capacity would make other dynamometer varieties impractical.

By using a way for measuring the rotational torque and angular speed by employing taper land hydrodynamic thrust bearing for measurement of the power of high engine performance is adopted in this project.

1-2 Classifications of Dynamometers

The Dynamometers may be classified as follow:

(a) Mechanical Brake Type Dynamometers.
(b) Hydraulic (Water Brake) Dynamometers.
(c) Eddy Current Dynamometers.
(d) AC and DC Dynamometers.
(e) Torque and Speed Measurement.

2. Development of Dynamometer Design

2-1 The Main Parts of the Dynamometer

Referring to **Fig.(1)**, the suggested design for the hydrodynameter consists the following essential part. These parts are:

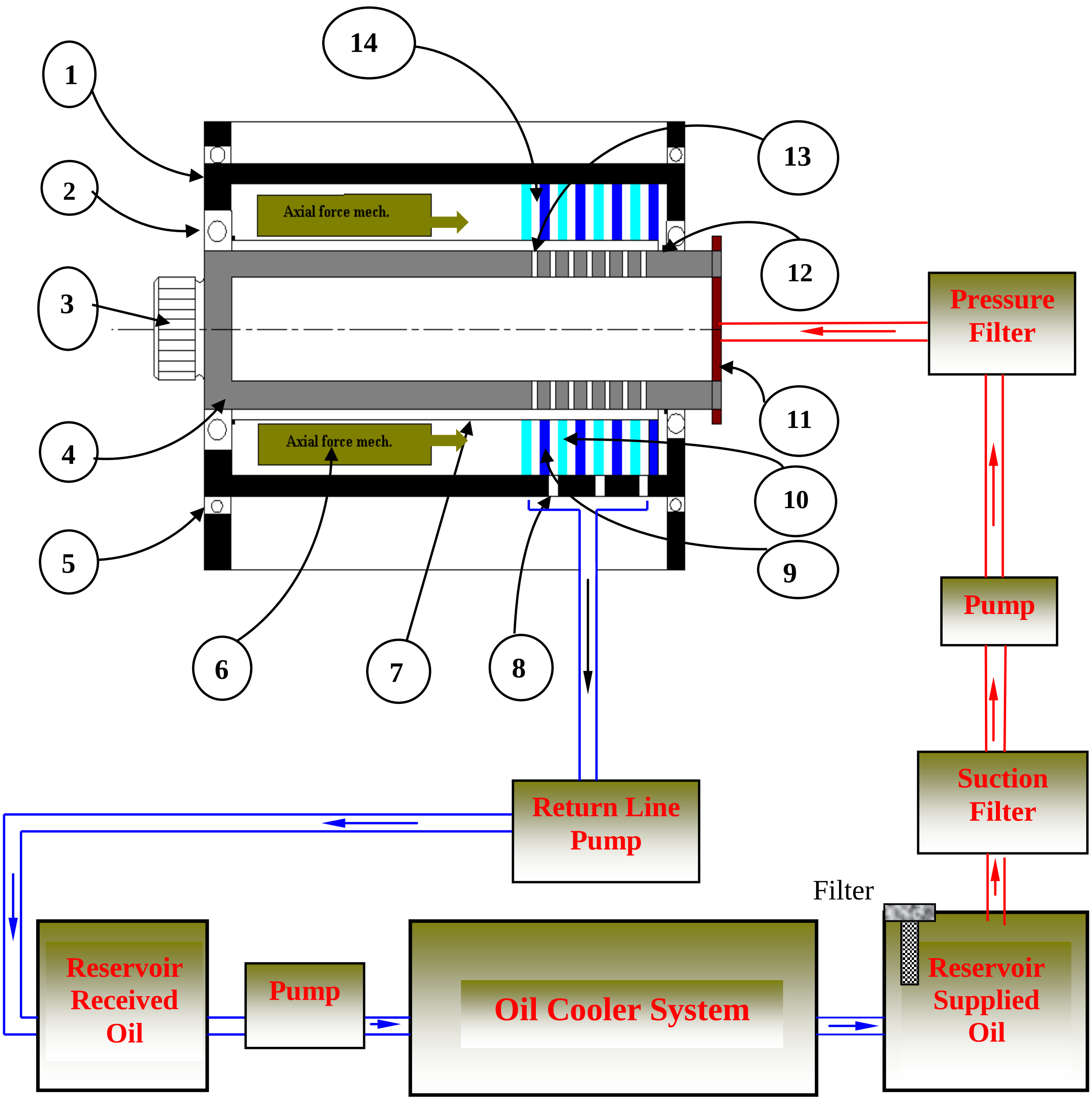

1- Housing
2- Shaft Bearing
3- Coupling
4- Hollow Shaft
5- Trunnion Bearing
6- Mechanism of Axial Force
7- Spline Tooth
8- Nine-Holes for Oil Outlet
9- Rotating Discs (Driver Discs)
10- Fixed Discs (Driven Discs)
11- Rotating Union
12- Carbon Face Seal
13- Holes for Oil Inlet
14- Oil-Film Generation

Figure (1) High power engine dynamometer assembly

2-1-1 Spline Shaft

The design of the splined shaft is achieved with a lot of care. Its design well studied from two sides. These two sides are stress analysis and dynamic performance (vibration and critical speed).

The aid of many references has been made, in order to get an ideal design. The following equations have been used in design, which is specific for the hollow shafts, Donald [3]:

$$D_o = \left[\frac{32 \cdot N_f}{\pi} \cdot \left(\frac{R^4}{R^4 - 1} \right) \cdot \sqrt{\left(\frac{M}{\sigma_e} \right)^2 + \frac{3}{4} \left(\frac{T}{\sigma_y} \right)^2} \right]^{1/3} \quad \text{..} \quad (1)$$

where:

$$\sigma_e = k_a \cdot k_b \cdot k_c \cdot k_d \cdot k_e \cdot k_f \cdot k_g \cdot \tilde{\sigma}_e$$

and for the dynamic performance the basic equation for the critical speed equation has been used, Gorman [4]. This equation is:

$$\omega_n = (\beta)^2 \cdot \sqrt{\frac{E \cdot I}{\rho \cdot L \cdot A^4}} \quad \text{...} \quad (2)$$

While in the numerical analysis, four models have been used. Referring to **Fig.(2)**, these models are:

- **A.** Hollow and splined along the whole length.
- **B.** Hollowed and splined along a part of the full length.
- **C.** Splined along a part of the full length and hollowed along the whole length.
- **D.** Splined and hollowed a long a part of the full length.

These four models have been solved using finite element facilities, which is ready program and ready package for usage.

Then the result was obtained and presented and discussed later.

2-1-2 Thrust Hydrodynamic Bearing (Taper Land Thrust Bearing)

The design of this bearing was based on Reynolds [5] equation. And this was simplified by [6], who listed the following design steps: modified to an empirical procedures by "Machinary's Handbook", and this part as considered is the heart of the dynamometer. This is because it performs the main function of the whole system.

Generally speaking, the bearing is usually used to separate the rotating parts from the stationary parts. And as a result it absorbs power, which is normally considered as disadvantages feature of the bearing. While in this application is used to absorb power. And the dynamometer is facilitated to measure this power. Therefore, instead of using couple mating discs {**Fig.(3)**} to support the axial load, (40) pairs of mating disks are used. These Fourty pairs works under the same axial load and as a result absorb power fourty times that absorbed by single pairs. The design procedures are [6]:

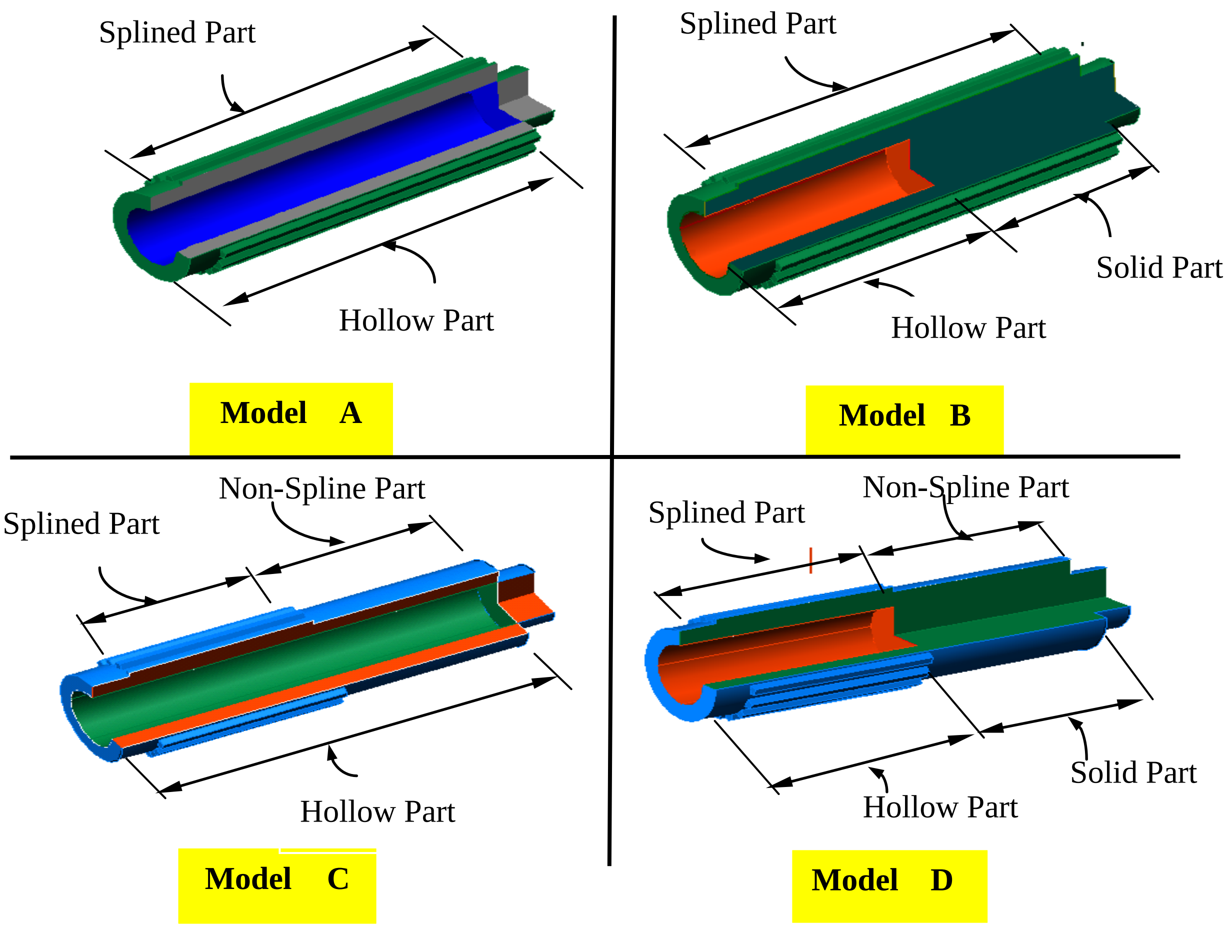

Figure (2) Spline shaft models

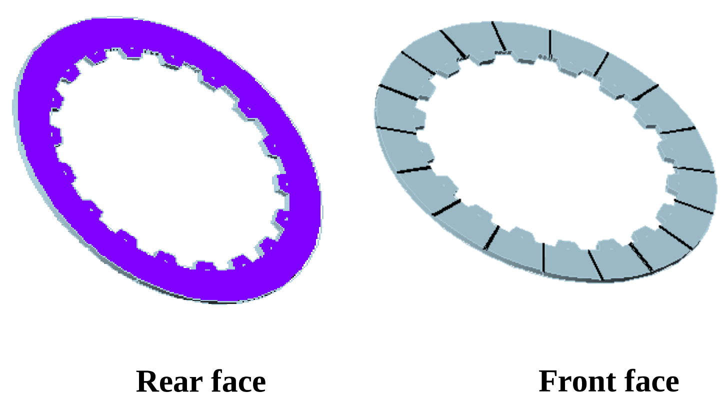

Figure (3) Thrust bearing of the dynamometer

$$d_o = \left(\frac{4 \cdot F_x}{\pi \cdot K_h \cdot p_{ul}} + d_i^2 \right)^{1/2} \quad \text{.......... (3)}$$

$$Y_L = \frac{B}{1 + \left(\pi^2 \cdot B^2 / 12 \cdot b^2 \right)} \quad \text{.......... (4)}$$

$$U = \frac{\pi}{24} \cdot (d_i + d_o) \cdot N \quad \text{.......... (5)}$$

$$p_{ul} = \frac{F_x}{i \cdot b \cdot B} \quad \text{.......... (6)}$$

$$K = \frac{p_{ul}}{6 \cdot \mu \cdot U \cdot Y_L} = 5.75 * 10^6 \cdot \frac{p_{ul}}{U \cdot Y_L \cdot Z} \quad \text{.......... (7)}$$

$$H_p = \frac{i \cdot b \cdot \mu \cdot B \cdot J \cdot U^2}{165000} = 8.79 * 10^{-3} \cdot i \cdot b \cdot B \cdot J \cdot U^2 \cdot Z \quad \text{.......... (8)}$$

$$Q_{re} = 42.4 \frac{H_p}{c_p . \Delta T} \quad \text{.......... (9)}$$

$$Y_s = \frac{8 \cdot b \cdot B}{d_o^2 - d_i^2} \quad \text{.......... (10)}$$

$$Q_{act} = \frac{8.9 * 10^{-4} \cdot i \cdot \delta_2 \cdot d_o^3 \cdot N \cdot Y_G \cdot Y_s^2}{d_o - d_i} \quad \text{.......... (11)}$$

Solving the above equations using a computer program gave the characteristics of the thrust bearing performance, such as, geometry and dimensions, power absorbed, oil flow rate ... etc. The obtained results will be discussed later in this report.

Also the thrust bearing was analyzed, regarding stresses. The stress state in rotating disc is analogous to a thick-wall cylinder under internal pressure, that due to centrifugal force which acts upon its distributed mass and attempts to pull it a part.

The tangential and radial stresses (σ_t, σ_r) of solid disc bearing as a function of its radius were calculated using the following equations, Robert [7].

$$\sigma_t = \frac{\gamma}{g} \cdot \omega^2 \cdot \left[\frac{3 + \upsilon}{8} \right] \cdot \left[r_i^2 + r_o^2 + \frac{r_i^2 \cdot r_o^2}{r} - \frac{1 + 3\upsilon}{3 + \upsilon} \cdot r^2 \right] \quad \text{.......... (12)}$$

And the radial stress is:

$$\sigma_r = \frac{\gamma}{g}\cdot\omega^2\cdot\left[\frac{3+\upsilon}{8}\right]\cdot\left[r_i^2 + r_o^2 + \frac{r_i^2\cdot r_o^2}{r} - r^2\right] \quad (13)$$

The stresses were calculated analytically using the above equations. And then calculated numerically using the ready package of finite element ANSYS.

2-1-3 Design of Oil Pumping and Cooling System

The design of the oil pumping and cooling system is based on the heat generated in the oil layers that used in the thrust bearing. This heat is generated due to shearing the oil layers due to rotation.

The heat calculation was based on the following equations [8]:

$$Q_t = m_t\cdot c_p\cdot(T_A - T_B) \quad (14)$$

$$Q_s = m_s\cdot c_p\cdot(T_C - T_D) \quad (15)$$

$$Q = \frac{1}{2}\cdot(Q_t + Q_s) \quad (16)$$

$$Q = U_i\cdot A_i\cdot\Delta T_m \quad (17)$$

$$\Delta T_m = \frac{(T_A - T_C) - (T_B - T_D)}{\ln\dfrac{T_A - T_C}{T_B - T_D}} \quad (18)$$

$$\Delta T_{me} = \Delta T_m\cdot Y \quad (19)$$

$$\frac{1}{U_i} = \frac{1}{h_t} + \frac{D_i}{2\cdot k_w}\cdot \mathrm{lin}\frac{D_o}{D_i} + \frac{D_i}{D_o} - \frac{1}{h_s} + F \quad (20)$$

Then a ready made heat exchanger was chosen, Holman and Frank [9,10]. These heat exchangers matches the heating requirements, that obtained by the previous equations.

3. Results and Discussion

3-1 Spline Shaft

3-1-1 Natural Frequency

Figures (4-7) show the relationship between natural frequency and the shaft diameter ratio for model A, B, C and D respectively (see section 1.2) and for different shaft lengths (where all the values of natural frequency taken for the first mode only).

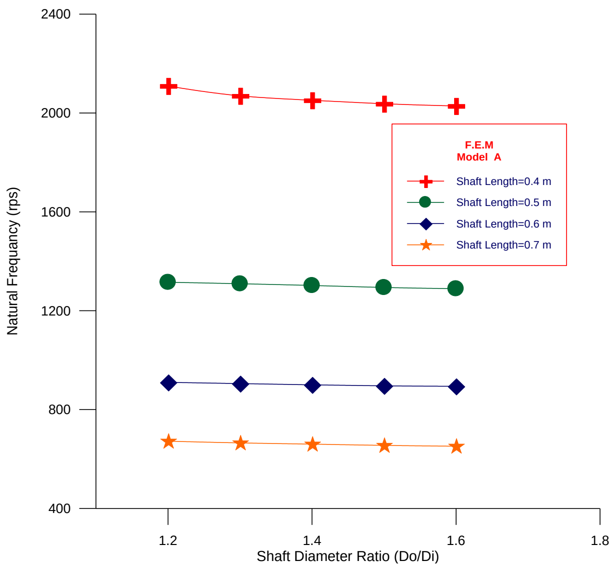

Figure (4) Relationship between natural frequency of spline shaft and shaft diameter ratio for model (A) for different shaft length by finite element method

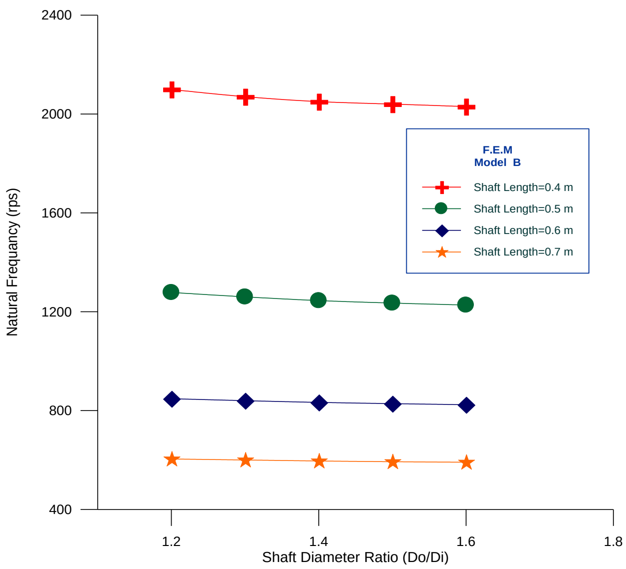

Figure (5) Relationship between natural frequency of spline shaft and shaft diameter ratio for model (B) for different shaft length by finite element method

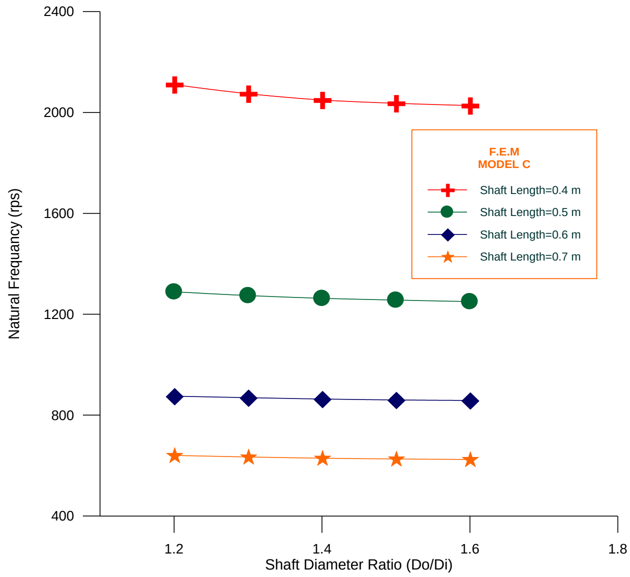

Figure (6) Relationship between natural frequency of spline shaft and shaft diameter ratio for model (C) for different shaft length by finite element method

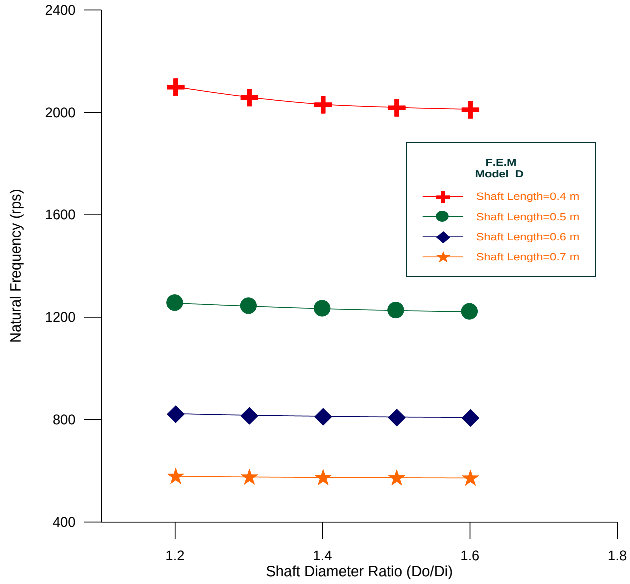

Figure (7) Relationship between natural frequency of spline shaft and shaft diameter ratio for model (D) for different shaft length by finite element method

These figures show that the natural frequency of the splined shaft is hardly affected by the diameter ratio D_o/D_i. But the more significant results that could be noticed, that the shaft length has a great influence on the natural frequency. And also it is noticed that for shaft length of 0.6 m the natural frequency is more acceptable practically if compared with the nominal rotational speed (which is equal to 15000 rpm in this work), and **Fig.(8)** shows that model A is the typical one.

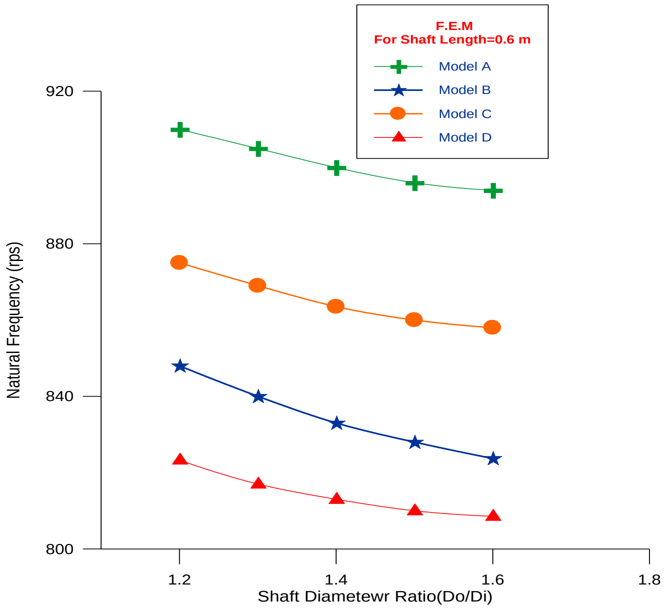

Figure (8) Relationship between natural frequencies of spline shaft and shaft diameter ratio for constant shaft length for models, A, B, C, and D for F.E.M.

Figure (9) shows the relationship between natural frequency and the shaft length for all four models of shaft design for the same shaft diameter ratio D_o/D_i which is equal to (1.5). And this shows how the numerical analysis could give more accurate results.

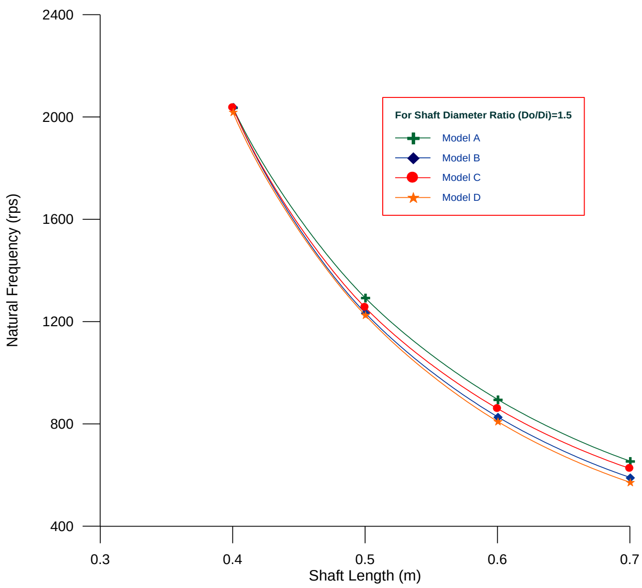

Figure (9) Relationship between natural frequencies of spline shaft and shaft length for constant diameter ratio for models, A, B, C, and D for F.E.M.

Figure (10) shows the bad influence of increasing the number of pairs on the natural frequency.

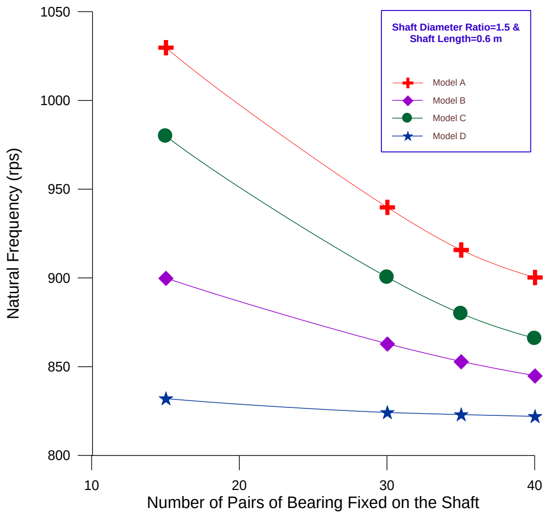

Figure (10) Relationship between natural frequencies of spline shaft and pairs of tapered-land thrust bearing for constants shaft length and diameter ratio for F.E.M for models A, B, C, and D

3-1-2 Stress Analysis

Figure (11) shows the contours of stresses (Von-Mises stresses) for four models under the following case study of shaft length is equal to 0.6 m and shaft diameter ratio D_o/D_i is equal to (1.5). It can be seen that the maximum value of stresses occurs at contact area between first pair and spline shaft and as far as from the first bearing pair the value of stresses decreases due to the increase of power absorbing by bearing pairs and that leads to decrease the transmitted torque.

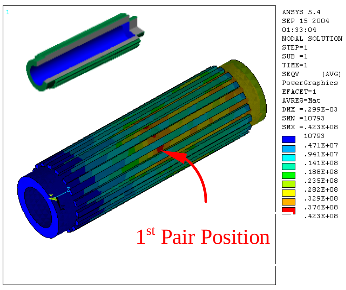

(a): Contour for Spline Shaft Model A

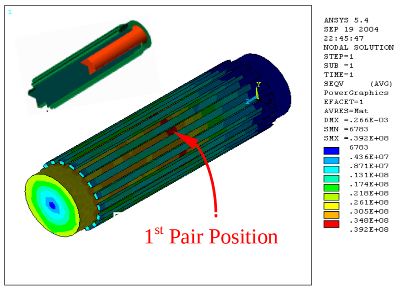

(b): Contour for Spline Shaft Models B

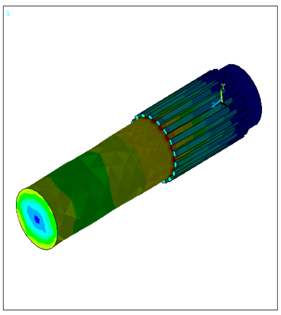

(c): Contour for Spline Shaft Models C

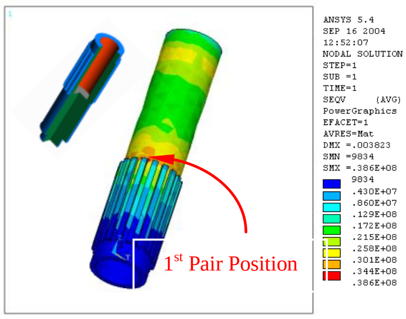

(d): Contour for Spline Shaft Models D

Figure (11) (a, b, c and d) Spline shaft contour for constant shaft length and diameter ratio, 0.6 m and 1.5 respectively for models A, B, C, and D

Figures (12-17) show the finite element results for the Von–Mises stresses against shaft diameter ration D_o/D_i for different shaft length and for model A, B, C and D respectively.

These figures show that the stresses decrease in a nonlinear relationship with the increase of shaft diameter ratio D_o/D_i due to the increase of the shaft cross section area and also the increase of its moment of inertia, which decreases the bending moment of the shaft.

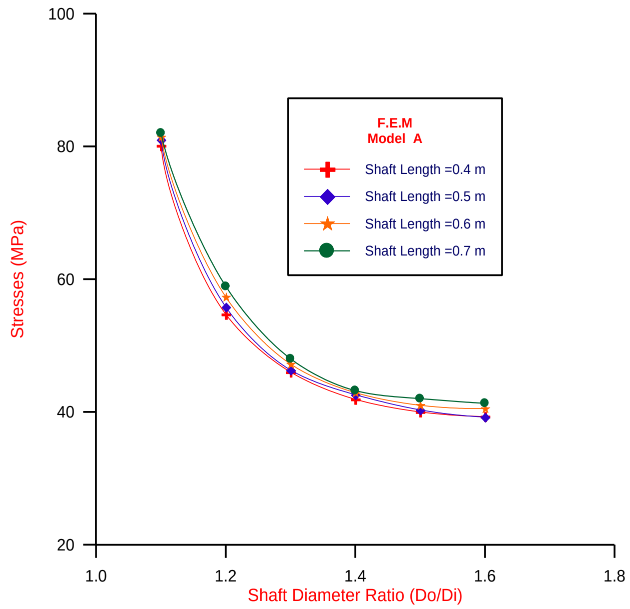

Figure (12) Relationship between Von-Mises stresses for spline shaft and shaft diameter ratio for model (A) or Finite Element Method

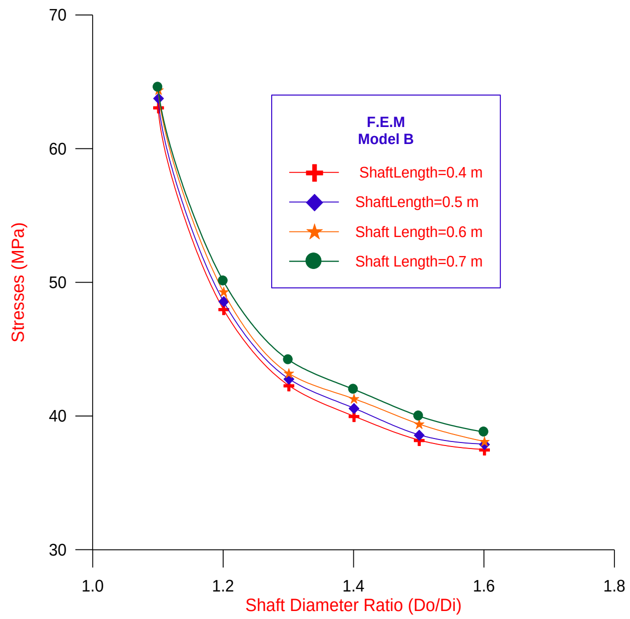

Figure (13) Relationship between Von-Mises stresses for spline shaft and shaft diameter for model (B) for Finite Element Method

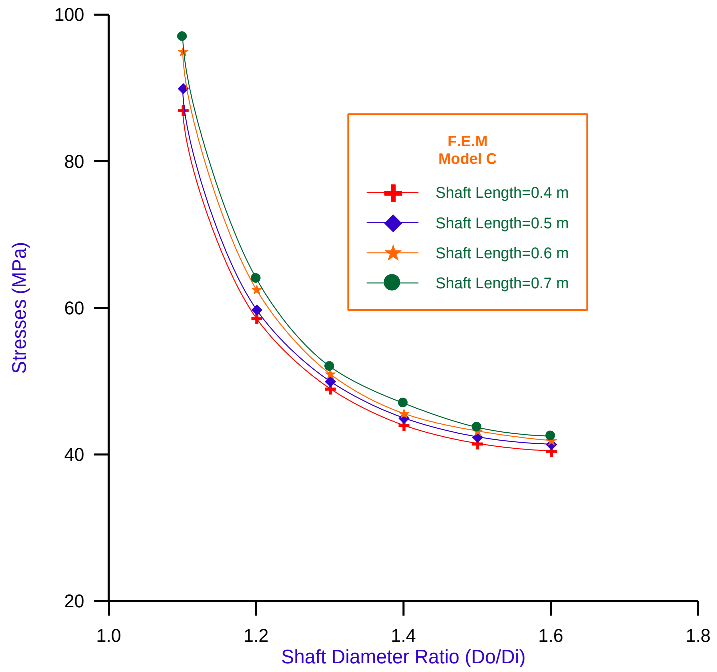

Figure (14) Relationship between Von-Mises stresses for spline shaft and shaft diameter ratio for model (C) for Finite Element Method

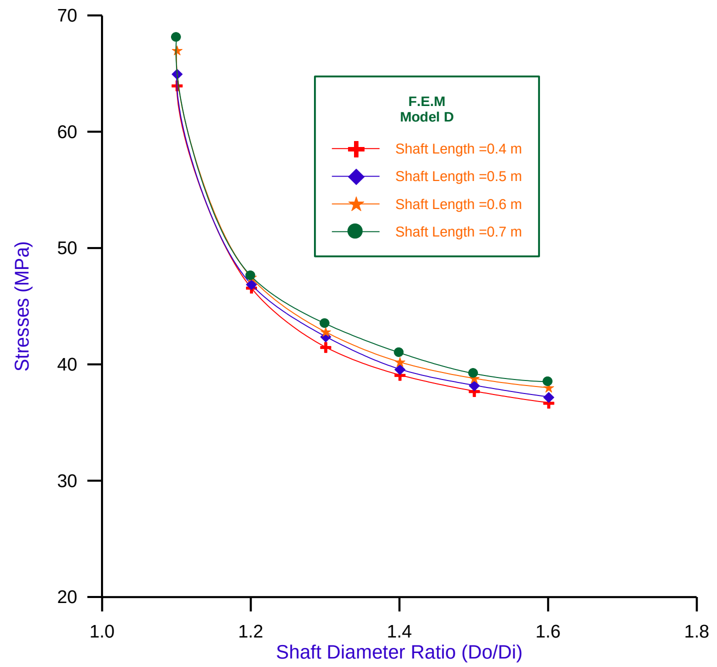

Figure (15) Relationship between Von-Mises stresses for spline shaft and shaft diameter ratio for model (D) for Finite Element Method

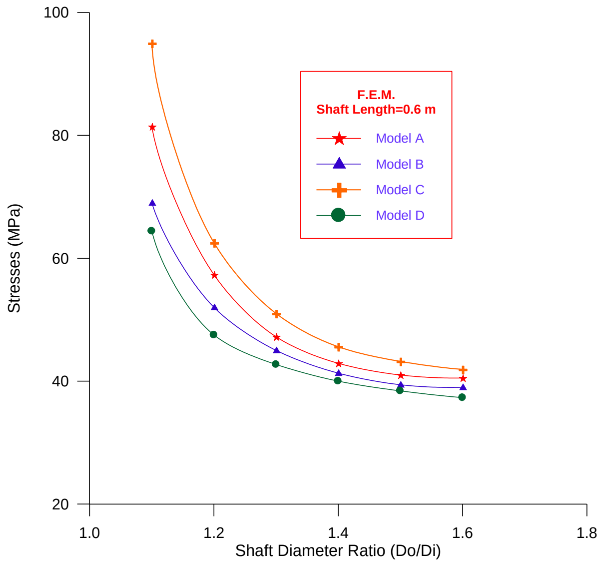

Figure (16) Relationship between Von-Mises stresses and shaft diameter ratio for spline shaft of constant length for modals A, B, C, and D

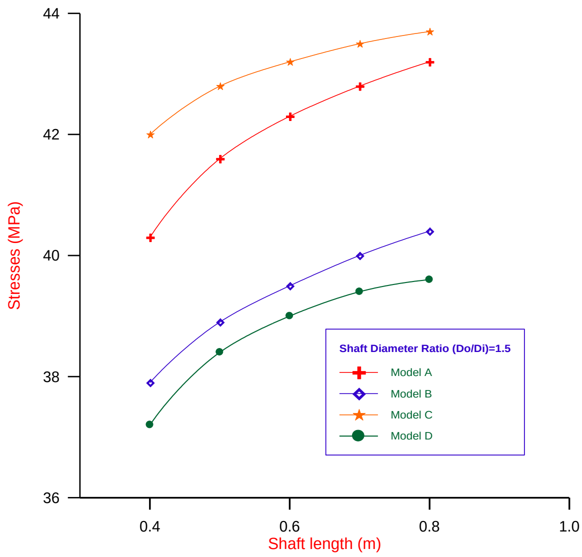

Figure (17) Relationship between Von-Mises stresses and shaft length for spline shaft of constant shaft diameter ratio for modals A, B, C, and D

Figure (16) shows the relationship between Von–Mises stresses and shaft diameter ratio D_o/D_i for shaft length (0.6 m) and for all four models.

It is clear from this figure that the stresses are higher values for model C compared with the other three models (A, B, and D) for any (D_o/D_i) ratio. Also this figure show that, for any model, the stress value is increased as the (D_o/D_i) ratio is decreased.

Figure (17) shows the relationship between Von–Mises stresses and the shaft length for the diameter ratio (1.5) and for all four models.

The figure illustrates that with the increase of shaft length the stresses of shaft increases in a nonlinear relationship due to the increase of bending moment of the spline shaft.

Figures (16 and 17) give acceptable values of stresses for spline shaft length equal to 0.6 m and shaft diameter ratio equal to 1.5 for model A, which have big difference if compared with yield strength. And this is considered compatible with the shaft designed.

3-2 Taper-Land Thrust Bearing

The solution steps are checked and compared with other workers methods of design, and were found in agreement. These workers are:

Michell [11], Dowson [12], Linn and Sheppard [13], Lord Rayleigh and Archibald [14].

3-2-1 Stresses Analysis by Finite Element

The thrust bearing that shown in **Fig.(18)** is analyzed using the finite element method in order to determine the tangential (hoop) stresses, and to know how the affects of variation of disc diameter on these stresses.

Pressure applied (for maximum engine power = 1660 kw (2225 hp) and angular speed =15000 rpm) = 11.25 ×107 N/m2 on each tooth face of bearing disc.

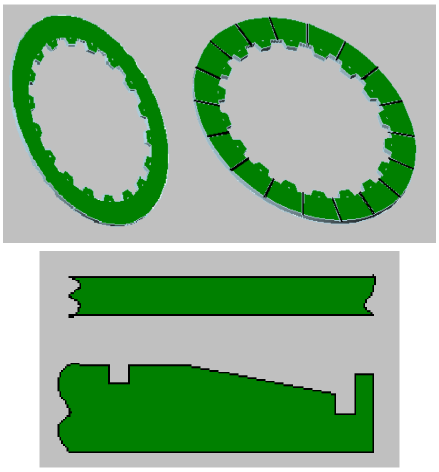

Figure (18) Tapered-Land thrust bearing

Figure (19) shows the relationship between tangential stresses and disc diameter ratio (do/di). And this illustrates how unnecessary increasing the disc diameter gives worse results on stress levels. And this could be seen from the figure that for the disc diameter ratio (1.14) gives (221Mpa). Hoop stresses where the disc diameter ratio of (1.5) gives (359Mpa). And these two stresses values are less than the yield strength of disc material, so it considered on the safe side.

Figure (20) shows the contours of the tangential stresses for different values of thrust bearing disc diameter ratio (do/di) = (1.14–1.5). This shows that the contours the maximum stresses occur at the teeth of the disc, i.e at the inner radius of the tapered land thrust bearing.

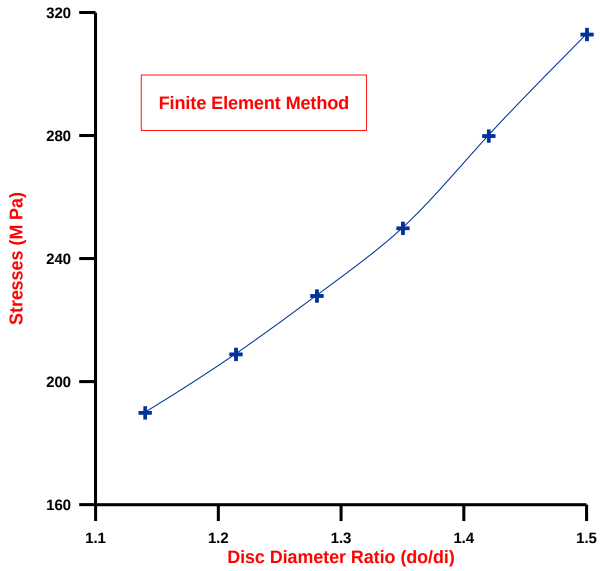

Figure (19) Relationship between hoop stresses and thrust bearing diameter ratio for F.E.M.

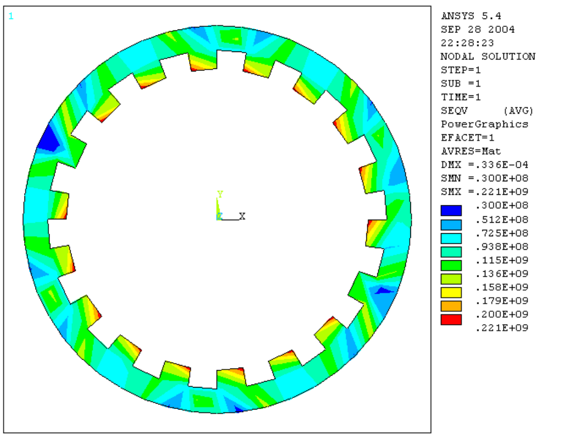

(a):Contour for disc with d_o/d_i =1.14

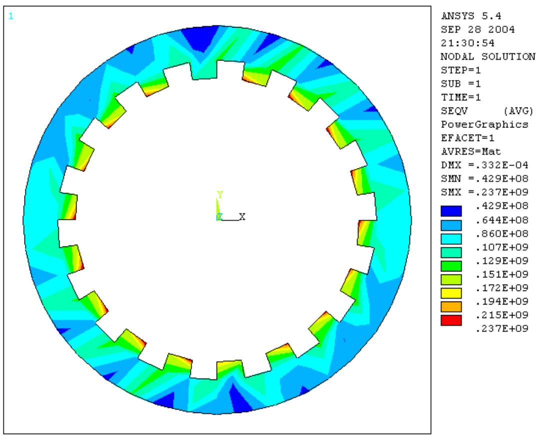

(b): Contour for disc with d_o/d_i =1.214

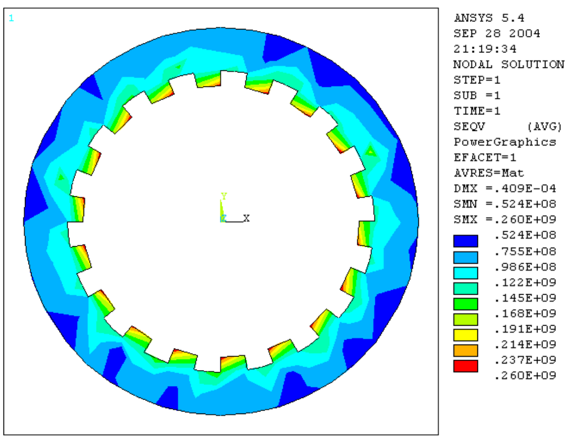

(c): Contour for disc with d_o/d_i =1.285

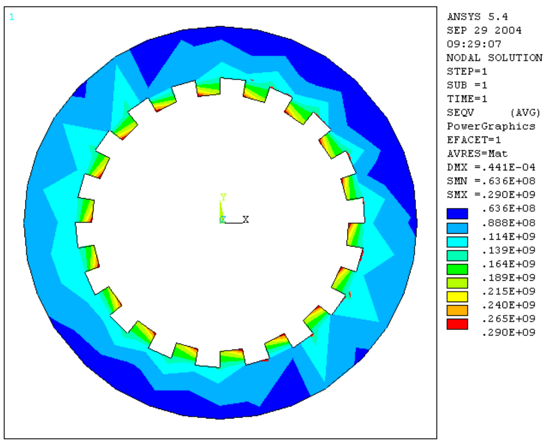

(d): Contour for disc with d_o/d_i =1.35

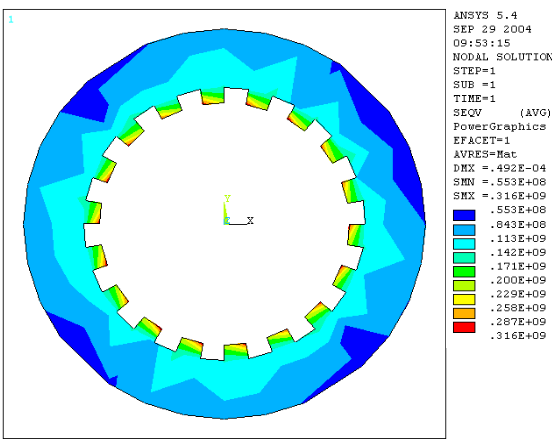

(e): Contour for disc with d_o/d_i =1.42

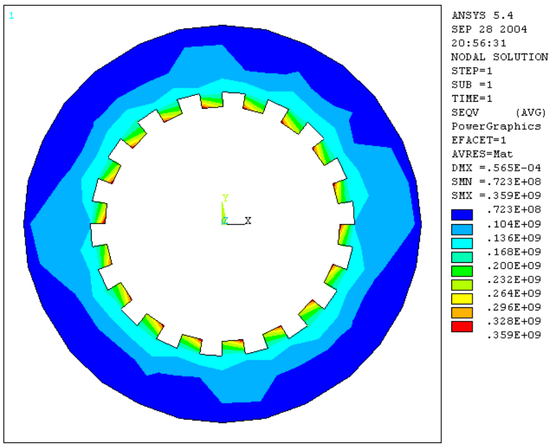

(f): Contour for disc with d_o/d_i =1.5

Figure (20) Tangential stress contours for taper-land thrust bearing for different diameter ratio d_o/d_i

4. Conclusions and Recommendations

4-1 Conclusions

The following conclusions have been drawn from the results.

1. Using the taper land thrust bearing to absorb torque and power and measuring them is considered a new method in designing of the hydraulic dynamometer.
2. Using the hydrodynamic thrust bearing for this purpose would not facilitate the dynamometer to apply zero torque.
3. The size of this type of dynamometer is relatively small compared with others of the commercial types.

4-2 Recommendations and Suggestions for Future Works

The following recommendations may be suggested:

a) Studying the types of mechanism that used for applying the axial load on the thrust bearing.
b) Studying the analysis of the other parts such as coupling, hub, and the base of the dynamometer.
c) Manufacture this dynamometer parts in order to carry out on experimental work that would reinforce thus theoretical work.

5. References

1. Land and Sea, ***"Dynamometer Comparison"***, Available Online at http://www.land-andsea.com/dynamometer/dynamometer-comparison.htm.

2. Taylor, C., and E., Taylor, ***"The Internal Combustion Engine"***, Scranton, International Text Book, 1961.

3. Donald A. Baker, ***"A Finite Element Study of Stresses in Steel Spline Shaft, and Partially Spline Shafts under Bending, Torsion, and Combined Loadings"***, M.Sc. Thesis, University of Virginia, May 2002.

4. Gorman, D. J., ***"Free Vibration Analysis of Beam and Shaft"***, John Wiley and Sons, 1975.

5. Reynolds, O., ***"Scientific Papers, V.II"***, Cambridge University Press, London, 1901.

6. ***"Machinery's Handbook"***, 20 Ed., Industrial Press Inc., 200 Mudison AVC, New York, N.Y. 10016, 1978.

7. Robert L. Norton, ***"Machine Design an Integrated Approach"***, Third Edition, McGraw Hill, 1999.

8. P., La Valle, and J. O., Wilkes, ***"Shell and Tube Heat Exchanger"***, Papers from Internet, December 16, 2003.

9. Holman, J. P., ***"Heat Transfer"***, Fourth Edition, McGraw Hill, 1976.

10. Frank Kreith, and Mark S. Bohn, ***"Principle of Heat Transfer"***, Sixth Edition, PWS Publishing Company, 2002.

11. Michell, A. G. M., ***"Tilting Pad Bearing and Their Practical Limitations"***, Proc. General Discussion on Lubrication and Lubricants, London (Reprinted by ASME, New York), 1968.

12. Dowson, R., ***"Thrust Bearing for Steam Turbine Machinery"***, Proc., General Discusion on Lubrication and Lubricants, London (Reprinted by ASME, New York), 1938.

13. Linn, F. C., and R., Sheppard, ***"The Tapered Land Thrust Bearing"***, Trans., Am., Soc., Mech., Engrs., 1938.

14. Rayleigh Lord, ***"Note on the Theory of Lubrication"***, Phil., Mag., 1918.

List of Symbols

Symbols	Definition	Units
A_i	Total tube inside area	m^2
A	Cross section area of the shaft	m^2
b	Radial width of each pad	m
B	Circumferential pad length at the pitch line	m
c_p	Specific heat of oil	J/kg. K
D	Solid shaft diameter	m
d_i	Inner diameter of the thrust bearing	m
D_i	Inner diameter of the hollow shaft	m
d_o	Outer diameter of the thrust bearing	m
D_o	Outer diameter of hollow shaft	m
E	Young's modules	N/m^2
F	fouling factor	
F_x	Thrust load	N
H_P	Power loss	W
h_s	the shell side heat transferred coefficient	
h_t	the tube side heat transferred coefficient	
i	number of pads	
I	Moment of inertia of the shaft	m^4
J	power loss coefficient	
K	Film thickness factor	
k_a, k_b, k_c, k_d, k_e, k_f, k_g	Factors for Surface, Size, Reliability, Temperature, Duty, fatigue and Miscellaneous respectively	
k_w	conductivity of tube wall	W/m.̊ c
K_h	Fraction of the circumference occupied by the pads	
L	Shaft length	m
M	Bending moment	N.m
m_s	Shell-side mass flow rate	kg/s
m_t	Tube-side mass flow rate	kg/s
N	Engine velocity	RPM
N_f	Factor of safety	
P_{ul}	Unit loading	N/m^2
Q_{act}	Actual oil flow	m^3/s
Q_{re}	Oil flow required	m^3/s
Q_s	The rate of heat transferred from shell side	W
Q_t	The rate of heat transferred from tube side	W
r	Radius	m
r_i, r_o	Inside and outside radii of the solid disk	m
R	Shaft diameter ratio	
T	Torque applied	N.m
T_A	Temperature entering tube	K
T_B	Temperature leaving tube	K
T_C	Temperature entering shell	K
T_D	Temperature leaving shell	K
U	Pitch line velocity	m/s

Symbols	Definition	Units
U_i	Overall heat transferred coefficient	$W/m^2\,K$
Y	Appropriate correction factor	
Y_G	Oil flow factor	
Y_L	Leakage factor	
Y_S	Shape factor	
Z	Oil viscosity	c.P
β	Frequency parameter	
γ	Material weight density, angular strain	N/m^3
δ_2	Tapered value at outer diameter	m
ΔT	Temperature difference	K
ΔT_m	Logarithmic mean temperature difference	K
ΔT_{me}	corrected logarithmic mean temperature difference	K
ν	Poisson's ratio	
ρ	Density	kg/m^3
σ_e	Corrected endurance limit	N/m^2
σ_t	Tangential stress	N/m^2
σ_r	Radial stress	N/m^2
σ_y	Yield strength	N/m^2
$\tilde{\sigma}_e$	Endurance limit of the test specimen	N/m^2
ω	Angular velocity	Rad/s
ω_n	Natural frequency	Rad/s
μ	Dynamic viscosity	reyns